

MONOCHROME AND COLOR POLARIZATION DEMOSAICKING USING EDGE-AWARE RESIDUAL INTERPOLATION

Miki Morimatsu, Yusuke Monno, Masayuki Tanaka, and Masatoshi Okutomi

Tokyo Institute of Technology, Tokyo, Japan

ABSTRACT

A division-of-focal-plane or microgrid image polarimeter enables us to acquire a set of polarization images in one shot. Since the polarimeter consists of an image sensor equipped with a monochrome or color polarization filter array (MPFA or CPFA), the demosaicking process to interpolate missing pixel values plays a crucial role in obtaining high-quality polarization images. In this paper, we propose a novel MPFA demosaicking method based on edge-aware residual interpolation (EARI) and also extend it to CPFA demosaicking. The key of EARI is a new edge detector for generating an effective guide image used to interpolate the missing pixel values. We also present a newly constructed full color-polarization image dataset captured using a 3-CCD camera and a rotating polarizer. Using the dataset, we experimentally demonstrate that our EARI-based method outperforms existing methods in MPFA and CPFA demosaicking.

Index Terms— Division-of-focal-plane polarimeter, polarization filter array, color-polarization image dataset, demosaicking.

1. INTRODUCTION

Polarization is a physical property of an electromagnetic wave such as light consisting of perpendicularly oscillating electric and magnetic fields [1]. Many studies have shown that polarization parameters, such as the angle of polarization (AoP) and the degree of polarization (DoP), are valuable for various image processing and computer vision applications, such as specular removal [2], reflection separation [3], and 3D shape reconstruction [4], to name a few.

Polarization images refer to a set of images acquired with different polarizer angles, from which polarization parameters are calculated for every pixel. Polarization images are typically captured by sequentially rotating a linear polarizer placed in front of a camera [5]. However, this conventional approach is not suitable for dynamic scenes and video acquisition, since it requires multiple shots for capturing a set of images.

As another approach, a division-of-focal-plane or microgrid image polarimeter acquires polarization images by using an image sensor equipped with a polarization filter array (PFA) [6]. A typical monochrome PFA (MPFA) consists of a 2×2 periodical pattern of four polarizers with angles of 0, 45, 90 and 135 degrees, respectively (see Fig. 1). Similarly, an image sensor equipped with the so-called quad-Bayer color PFA (CPFA, see Fig. 2) is recently produced by Sony with a much-reduced price from existing color-

polarization sensors [7]. These PFA-based sensors are suitable for dynamic scenes and video capturing, since they enable one-shot acquisition of monochrome or color polarization pixel values. For the PFA-based sensors, the demosaicking, which is an interpolation process of missing polarization pixel values, is the key component in acquiring high-quality polarization images.

Many demosaicking methods have been proposed for MPFA, including interpolation-based [8–15] (see [6] for a survey), dictionary-based [16], and deep learning-based methods [17]. Recently, a few methods have also been proposed for CPFA based on the reconstruction-based [18] or deep learning-based approach [19]. Although learning-based methods [16, 17, 19] generally achieve higher performance than interpolation-based methods, they are highly data-dependent and require a large amount of training images, which remain difficult to be collected for non-RGB images. They also require high computational time [16] or large memory size [17, 19], which is not desirable for integrated sensor systems.

In this paper, we propose a novel MPFA demosaicking method based on residual interpolation (RI) [20] and also extend that method to CPFA demosaicking. RI is one of high-performance interpolation methods based on a guide image and has shown its superiority in color demosaicking [20–25]. Although RI has also been applied to MPFA demosaicking in some methods [6, 13–15], they do not fully consider the edge information to generate the guide image. In contrast, we propose a novel *edge-aware* RI (EWRI) by incorporating a new edge detector to effectively generate a better guide image.

One limitation of MPFA and CPFA demosaicking research is the lack of evaluation datasets. Although some recent papers have presented the construction of a color-polarization image dataset, it is captured by a Bayer-patterned camera [18, 26] or has not yet published [18, 19]. Thus, we constructed a new full 12-channel color-polarization image dataset with 40 scenes¹ by using a 3-CCD RGB camera and a polarizer rotated with four orientations. Experimental results using the new dataset demonstrate that our EARI-based method outperforms the best-performed existing interpolation-based method in the recent survey paper [6].

2. PROPOSED METHOD

2.1. Proposed MPFA demosaicking method

Figure 1 shows the outline of our proposed MPFA demosaicking method based on EARI. We apply RI [21], which is an interpolation method based on a guide image, to interpolate missing pixel values in each polarization orientation. To generate an effective guide image, we propose a novel guide image generation manner considering four-directional intensity and polarization edges. Each processing step is detailed below.

¹The dataset and the source code of our proposed method are publicly available at <http://www.ok.sc.e.titech.ac.jp/res/PolarDem/index.html>.

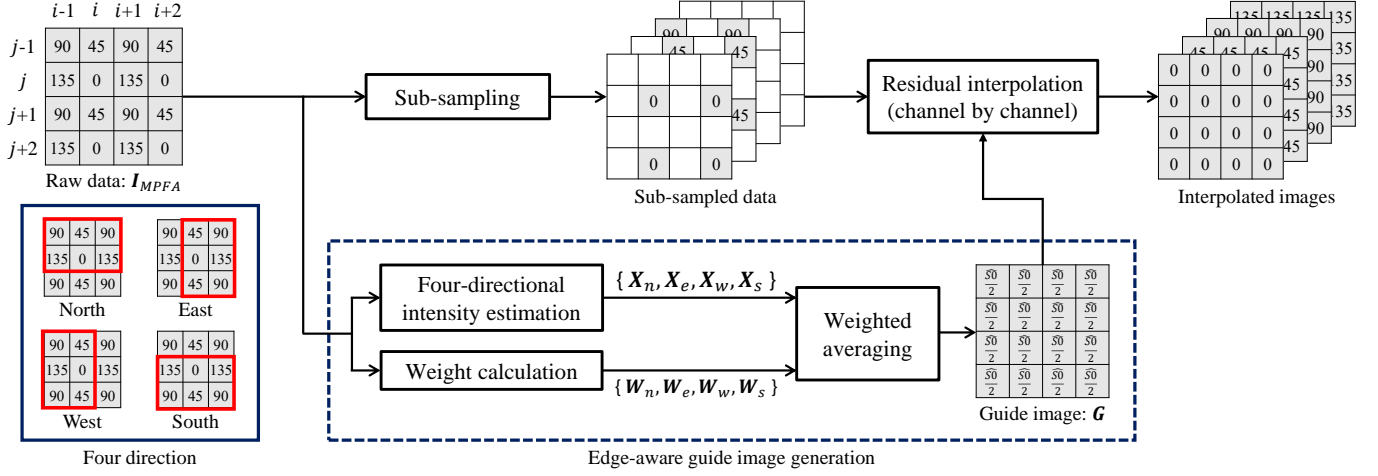


Fig. 1. The outline of our proposed MPFA demosaicking method based on EARI

We generate the guide image G from raw MPFA data I_{MPFA} by estimating four-directional intensity images and averaging them based on the weights for each direction. By definition, the intensity S_0 , which is one of the Stokes polarization parameters [1], is expressed as

$$S_0 = I_0 + I_{90} = I_{45} + I_{135}, \quad (1)$$

where I_0, I_{45}, I_{90} , and I_{135} are the associated pixel values of the images at four polarization orientations, respectively.

We explain our idea of four-directional estimation, which is inspired by the horizontal-vertical edge detector of [11], by taking the intensity estimation at pixel (i, j) in the north direction (see Fig. 1) as example. Based on the definition of Eq. (1), for the north region, we estimate the intensity of pixel (i, j) by two ways as

$$\begin{aligned} \widehat{S}_{0_{n(0,90)}}(i, j) &= I_0(i, j) + \frac{1}{2}[I_{90}(i-1, j-1) + I_{90}(i+1, j-1)], \\ \widehat{S}_{0_{n(45,135)}}(i, j) &= I_{45}(i, j-1) + \frac{1}{2}[I_{135}(i-1, j) + I_{135}(i+1, j)], \end{aligned} \quad (2)$$

where suffix n represents the north region, $\widehat{S}_{0_{n(0,90)}}$ and $\widehat{S}_{0_{n(45,135)}}$ are the estimated intensities using (I_0, I_{90}) and (I_{45}, I_{135}) , respectively. We then calculate the average and the difference of the two estimates as

$$\widehat{S}_{0_n}(i, j) = \frac{1}{2}[\widehat{S}_{0_{n(0,90)}}(i, j) + \widehat{S}_{0_{n(45,135)}}(i, j)], \quad (3)$$

$$\Delta\widehat{S}_{0_n}(i, j) = \widehat{S}_{0_{n(0,90)}}(i, j) - \widehat{S}_{0_{n(45,135)}}(i, j). \quad (4)$$

If there are no intensity edges and polarization edges (i.e., edges caused by the polarization parameter differences between pixels) in the region, the difference of Eq. (4) becomes zero, meaning that the intensity of Eq. (3) is estimated without crossing the edges. Thus, we evaluate the intensity differences for four directions (i.e., north, east, west, and south in Fig. 1) to determine the weights of interpolation directions for generating an edge-aware guide image.

The four-directional intensity estimates and intensity differences can be calculated by filtering the raw MPFA data I_{MPFA} . The directional intensity estimate $X_k = \widehat{S}_{0_k}/2$, which is normalized to the pixel value range, is calculated as

$$X_k = F_k \otimes I_{MPFA}, \quad k = \{n, e, w, s\}, \quad (5)$$

where \otimes represents the filtering operation and k represents the direction of north (n), east (e), west (w), and south (s). F_k is the filter

kernel for k -direction, which is expressed as

$$\begin{aligned} F_n &= \begin{bmatrix} 1/8 & 1/4 & 1/8 \\ 1/8 & 1/4 & 1/8 \\ 0 & 0 & 0 \end{bmatrix}, F_e = \begin{bmatrix} 0 & 1/8 & 1/8 \\ 0 & 1/4 & 1/4 \\ 0 & 1/8 & 1/8 \end{bmatrix}, \\ F_w &= \begin{bmatrix} 1/8 & 1/8 & 0 \\ 1/4 & 1/4 & 0 \\ 1/8 & 1/8 & 0 \end{bmatrix}, F_s = \begin{bmatrix} 0 & 0 & 0 \\ 1/8 & 1/4 & 1/8 \\ 1/8 & 1/4 & 1/8 \end{bmatrix}. \end{aligned} \quad (6)$$

The directional intensity difference $\Delta\widehat{S}_{0_k}$ is calculated as

$$\Delta\widehat{S}_{0_k} = H_k \otimes I_{MPFA}, \quad k = \{n, e, w, s\}, \quad (7)$$

where each filter kernel H_k is expressed as

$$\begin{aligned} H_n &= \begin{bmatrix} -1/2 & 1 & -1/2 \\ 1/2 & -1 & 1/2 \\ 0 & 0 & 0 \end{bmatrix}, H_e = \begin{bmatrix} 0 & 1/2 & 1/2 \\ 0 & -1 & 1 \\ 0 & 1/2 & -1/2 \end{bmatrix}, \\ H_w &= \begin{bmatrix} -1/2 & 1/2 & 0 \\ 1 & -1 & 0 \\ -1/2 & 1/2 & 0 \end{bmatrix}, H_s = \begin{bmatrix} 0 & 0 & 0 \\ 1/2 & -1 & 1/2 \\ -1/2 & 1 & -1/2 \end{bmatrix}. \end{aligned} \quad (8)$$

We then calculate the weight for each direction as

$$W_k(i, j) = \frac{1}{\Delta\widehat{S}'_{0_k}(i, j) + \varepsilon}, \quad (9)$$

$$\Delta\widehat{S}'_{0_k} = M_k \otimes |\Delta\widehat{S}_{0_k}| \quad (10)$$

where M_k is the 5×5 -sized smoothing kernel for k -direction, ε is a small positive value (set as 10^{-32}) to avoid the division by zero, and $|\cdot|$ represents the element-wise absolute value operator.

The edge-aware guide image G is then generated by the pixel-wise weighted averaging of $X_k(i, j)$ as

$$G(i, j) = \sum_{k=n,e,w,s} W_k(i, j) X_k(i, j) / \sum_{k=n,e,w,s} W_k(i, j). \quad (11)$$

Using the generated guide image, we finally apply RI [21] to interpolate missing pixel values at each polarization orientation.

2.2. Extension to CPFA demosaicking

We here extend our proposed MPFA demosaicking method to CPFA demosaicking. Figure 2 shows the outline of our proposed CPFA

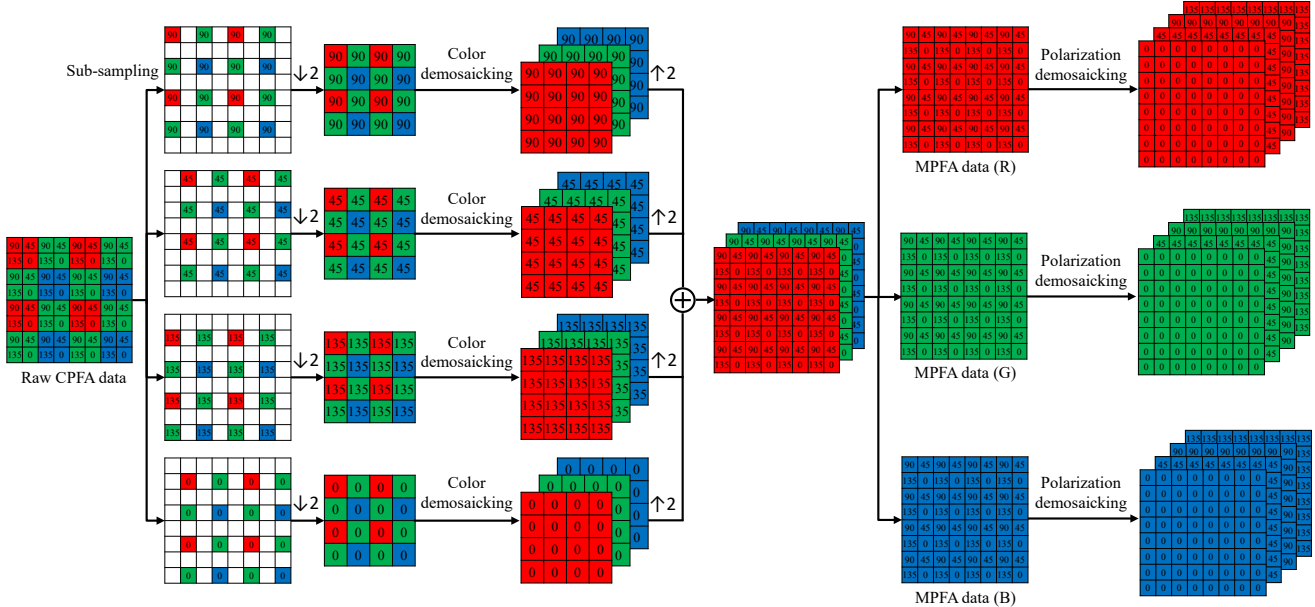


Fig. 2. The outline of our proposed CPFA demosaicking framework

demosaicking framework, which effectively combines existing color and our MPFA demosaicking methods. We first sub-sample and down-sample (as expressed by $\downarrow 2$) the raw CPFA data to obtain Bayer-patterned data of four orientations. We then apply an existing color demosaicking method to each Bayer-patterned data. The four demosaicked RGB images are then up-sampled (as expressed by $\uparrow 2$) and aligned to form the MPFA data of each color channel. Finally, we apply our MPFA demosaicking method to each MPFA data to obtain full 12-channel color-polarization images.

3. COLOR-POLARIZATION IMAGE DATASET

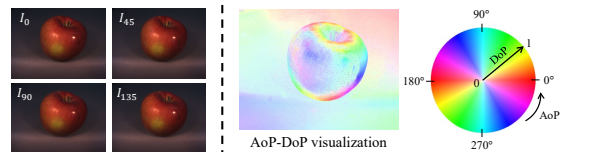
We newly constructed the full 12-channel color-polarization image dataset with 40 scenes, as shown in Fig. 3. Each 12-channel data consists of four RGB images captured with four polarizer angles of 0, 45, 90, and 135 degrees, as shown in Fig. 3(a). We used JAI CV-M9GE 3-CCD camera, and SIGMAKOKI SPF-50C-32 linear polarizer attached to PH-50-ARS rotating polarizer mount. Each 12-channel data was captured by rotating the linear polarizer placed in front of the camera under an unpolarized light condition. For each polarizer orientation, we captured 1,000 images and averaged them to make the ground-truth image with reduced noise, as performed in [27]. The image resolution is 1024×768 with 10-bit depth.

4. EXPERIMENTAL RESULTS

4.1. MPFA demosaicking results

We evaluated the performance of our MPFA demosaicking method using the green-channel images of our color-polarization dataset as ground-truth monochrome polarization images. We compared our EARI-based method with four interpolation-based methods: bilinear, bicubic, ICPC [11], and PPID [6]. The PPID method is also based on a guide image called a pseudo-panchromatic image [28] and presents the best performance in the recent survey paper [6].

Table 1 shows the average angle RMSE (RMSE of the angle errors) for AoP images and the average PSNR for four polarization



(a) Example color-polarization image set and its AoP-DoP visualization



(b) 40 scenes in the dataset

Fig. 3. Our full 12-channel color-polarization image dataset

images (I_0 , I_{45} , I_{90} , and I_{135}), three Stokes parameter images (S_0 , S_1 , S_2), and DoP images. A higher PSNR value and a lower angle error mean better performance. We can see that our EARI outperforms state-of-the-art PPID in most parameters. The bottom row in the table is the RI method using a non-edge-aware guide image generated by a simple non-directional 3×3 averaging filter. We can clearly confirm that, compared with non-directional RI, EARI improves the performance by generating the edge-aware guide image. Figure 4 shows the visual comparison of selected methods (see the supplemental material for the results of all methods), where the S_0 image and the AoP-DoP visualization of Fig. 3(a) are presented. We can see that our EARI generates a better result without color edge artifact as in ICPC and zipper artifacts as in PPID.

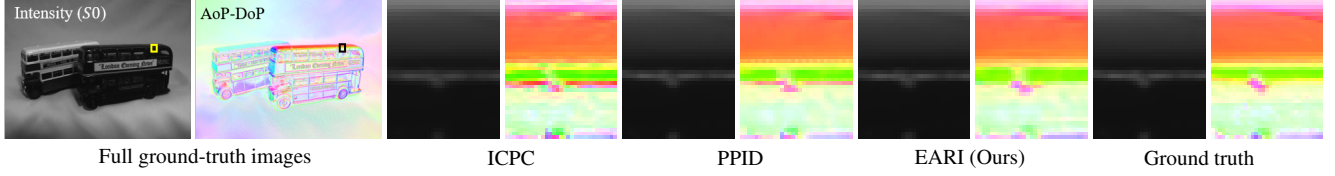


Fig. 4. Visual comparison of the intensity image and the AoP-DoP visualization for MPFA demosaicking

Table 1. Numerical comparison for MPFA demosaicking (Average of 40 scenes)

Method	PSNR								Angle error	
	I_0	I_{45}	I_{90}	I_{135}	S_0	S_1	S_2	DoP	AoP	
Bilinear	42.34	41.58	42.50	41.58	44.89	46.14	45.03	33.70	21.36	
Bicubic	43.45	42.48	43.63	42.48	46.22	47.00	45.73	34.46	20.64	
ICPC [11]	43.10	42.22	43.23	42.22	45.78	47.01	45.73	34.75	20.50	
PPID [6]	46.52	44.52	46.91	44.34	48.94	50.56	47.59	36.96	17.65	
EARI (Ours)	47.39	44.91	47.84	44.63	49.62	51.48	47.83	36.79	17.13	
non-edge-aware	47.01	44.68	47.41	44.46	49.27	51.02	47.70	36.25	17.44	

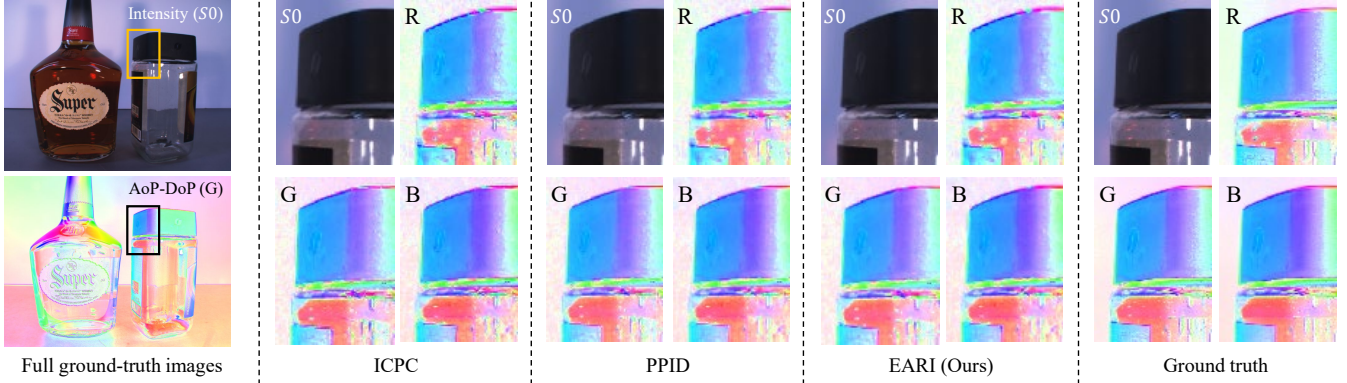


Fig. 5. Visual comparison of the intensity image and the AoP-DoP visualization for CPFA demosaicking

Table 2. Numerical comparison for CPFA demosaicking (Average of 40 scenes)

Method		CPSNR								Angle error	
(color polarization)		I_0	I_{45}	I_{90}	I_{135}	S_0	S_1	S_2	DoP	AoP	
Bilinear		35.32	34.94	35.47	35.00	36.31	43.29	41.28	31.20	24.98	
RI	Bilinear	38.34	37.79	38.50	37.86	40.03	44.09	42.58	31.96	24.15	
	Bicubic	38.65	38.05	38.81	38.12	40.43	44.30	42.72	32.05	24.11	
	ICPC [11]	38.61	38.01	38.77	38.09	40.33	44.49	42.87	32.36	23.86	
	PPID [6]	39.37	38.68	39.57	38.71	40.73	46.34	44.04	33.98	22.40	
	EARI (Ours)	39.41	38.72	39.62	38.72	40.76	46.49	44.10	33.74	22.18	
	non-edge-aware	39.35	38.65	39.55	38.67	40.73	46.28	43.97	33.36	22.32	

4.2. CPFA demosaicking results

We next evaluated the performance of CPFA demosaicking using our full 12-channel color-polarization image dataset. We applied minimized-Laplacian RI [21] for the color demosaicking step and compared our EARI with the same MPFA demosaicking methods as presented before. We also compared bilinear interpolation applied to each of the sparse 12-channel data as the most basic method.

Table 2 shows the average color PSNR (CPSNR) and the average angle RMSE (the average of RGB) for CPFA demosaicking. Similar to the MPFA demosaicking, we can confirm that our EARI provides better performance compared with PPID and also demonstrates the improvement compared with the non-directional RI. In the visual comparison of Fig. 5 (see the supplemental material for the results

of all methods), our EARI shows the slightly better results on the top of the bin lid, though there still exists jaggy artifacts, since the CPFA demosaicking is very challenging due to the very sparse nature of each color-polarization sample.

5. CONCLUSION

In this paper, we have proposed a novel MPFA demosaicking method based on newly proposed EARI, where we generate the guide image in an edge-aware manner to effectively interpolate missing pixel values without crossing the edges. We also have proposed a CPFA demosaicking framework that effectively combines existing color and our MPFA demosaicking methods. To evaluate the demo-

saicking performance, we have constructed a new full 12-channel color-polarization image dataset. Using the dataset, we experimentally demonstrate that our EARI-based method achieves better performance than existing methods in both MPFA and CPFA demosaicking. Future work includes the consideration of noise and the proposal of a joint denoising and demosaicking method.

Acknowledgment. We would like to thank Dr. Sofiane Mihoubi and Dr. Pierre-Jean Lapray for sharing the executable code of the PPID method.

6. REFERENCES

- [1] Edward Collett, *Field guide to polarization*, SPIE, 2005.
- [2] Laurent Valentin Jospin, Gilles Baechler, and Adam Scholefield, "Embedded polarizing filters to separate diffuse and specular reflection," *Proc. of Asian Conf. on Computer Vision (ACCV)*, pp. 3–18, 2018.
- [3] Patrick Wieschollek, Orazio Gallo, Jinwei Gu, and Jan Kautz, "Separating reflection and transmission images in the wild," *Proc. of European Conf. on Computer Vision (ECCV)*, pp. 89–104, 2018.
- [4] Zhaopeng Cui, Jinwei Gu, Boxin Shi, Ping Tan, and Jan Kautz, "Polarimetric multi-view stereo," *Proc. of IEEE Conf. on Computer Vision and Pattern Recognition (CVPR)*, pp. 1558–1567, 2017.
- [5] J Scott Tyo, Dennis L Goldstein, David B Chenault, and Joseph A Shaw, "Review of passive imaging polarimetry for remote sensing applications," *Applied Optics*, vol. 45, no. 22, pp. 5453–5469, 2006.
- [6] Sofiane Mihoubi, Pierre-Jean Lapray, and Laurent Bigué, "Survey of demosaicking methods for polarization filter array images," *Sensors*, vol. 18, no. 11, pp. 3688, 2018.
- [7] Yasushi Maruyama, Takashi Terada, Tomohiro Yamazaki, Yusuke Uesaka, Motoaki Nakamura, Yoshihisa Matoba, Kenta Komori, Yoshiyuki Ohba, Shinichi Arakawa, Yasutaka Hirasawa, Yuhi Kondo, Jun Murayama, Kentaro Akiyama, Yusuke Oike, Shuzo Sato, and Takayuki Ezaki, "3.2-MP back-illuminated polarization image sensor with four-directional air-gap wire grid and 2.5- μm pixels," *IEEE Trans. on Electron Devices*, vol. 65, no. 6, pp. 2544–2551, 2018.
- [8] Bradley M. Ratliff, Charles F. LaCasse, and J. Scott Tyo, "Interpolation strategies for reducing IFOV artifacts in microgrid polarimeter imagery," *Optics Express*, vol. 17, no. 11, pp. 9112–9125, 2009.
- [9] Shengkui Gao and Viktor Gruev, "Bilinear and bicubic interpolation methods for division of focal plane polarimeters," *Optics Express*, vol. 19, no. 27, pp. 26161–26173, 2011.
- [10] Shengkui Gao and Viktor Gruev, "Gradient-based interpolation method for division-of-focal-plane polarimeters," *Optics Express*, vol. 21, no. 1, pp. 1137–1151, 2013.
- [11] Junchao Zhang, Haibo Luo, Bin Hui, and Zheng Chang, "Image interpolation for division of focal plane polarimeters with intensity correlation," *Optics Express*, vol. 24, no. 18, pp. 20799–20807, 2016.
- [12] Ning Li, Yongqiang Zhao, Quan Pan, and Seong G Kong, "Demosaicking DoFP images using Newtons polynomial interpolation and polarization difference model," *Optics Express*, vol. 27, no. 2, pp. 1376–1391, 2019.
- [13] Ashfaq Ahmed, Xiaojin Zhao, Viktor Gruev, Junchao Zhang, and Amine Bermak, "Residual interpolation for division of focal plane polarization image sensors," *Optics Express*, vol. 25, no. 9, pp. 10651–10662, 2017.
- [14] Ashfaq Ahmed, Xiaojin Zhao, Jintao Chang, Hui Ma, Viktor Gruev, and Amine Bermak, "Four-directional adaptive residual interpolation technique for DoFP polarimeters with different micro-polarizer patterns," *IEEE Sensors Journal*, vol. 18, no. 19, pp. 7990–7997, 2018.
- [15] Tuochi Jiang, Desheng Wen, Zongxi Song, Weikang Zhang, Zhixin Li, Xin Wei, and Gang Liu, "Minimized Laplacian residual interpolation for DoFP polarization image demosaicking," *Applied Optics*, vol. 58, no. 27, pp. 7367–7374, 2019.
- [16] Junchao Zhang, Haibo Luo, Rongguang Liang, Ashfaq Ahmed, Xiangyue Zhang, Bin Hui, and Zheng Chang, "Sparse representation-based demosaicking method for microgrid polarimeter imagery," *Optics Letters*, vol. 43, no. 14, pp. 3265–3268, 2018.
- [17] Junchao Zhang, Jianbo Shao, Haibo Luo, Xiangyue Zhang, Bin Hui, Zheng Chang, and Rongguang Liang, "Learning a convolutional demosaicking network for microgrid polarimeter imagery," *Optics Letters*, vol. 43, no. 18, pp. 4534–4537, 2018.
- [18] Simeng Qiu, Qiang Fu, Congli Wang, and Wolfgang Heidrich, "Polarization demosaicking for monochrome and color polarization focal plane arrays," *Proc. of Int. Symposium on Vision, Modeling, and Visualization (VMV)*, pp. 117–124, 2019.
- [19] Sijia Wen, Yinqiang Zheng, Feng Lu, and Qinqing Zhao, "Convolutional demosaicking network for joint chromatic and polarimetric imagery," *Optics Letters*, vol. 44, no. 22, pp. 5646–5649, 2019.
- [20] Daisuke Kiku, Yusuke Monno, Masayuki Tanaka, and Masatoshi Okutomi, "Residual interpolation for color image demosaicking," *Proc. of IEEE Int. Conf. on Image Processing (ICIP)*, pp. 2304–2308, 2013.
- [21] Daisuke Kiku, Yusuke Monno, Masayuki Tanaka, and Masatoshi Okutomi, "Beyond color difference: Residual interpolation for color image demosaicking," *IEEE Trans. on Image Processing*, vol. 25, no. 3, pp. 1288–1300, 2016.
- [22] Wei Ye and Kai-Kuang Ma, "Color image demosaicking using iterative residual interpolation," *IEEE Trans. on Image Processing*, vol. 24, no. 12, pp. 5879–5891, 2015.
- [23] Yonghoon Kim and Jechang Jeong, "Four-direction residual interpolation for demosaicking," *IEEE Trans. on Circuits and Systems for Video Technology*, vol. 26, no. 5, pp. 881–890, 2015.
- [24] Yusuke Monno, Daisuke Kiku, Masayuki Tanaka, and Masatoshi Okutomi, "Adaptive residual interpolation for color image demosaicking," *Proc. of IEEE Int. Conf. on Image Processing (ICIP)*, pp. 3861–3865, 2015.
- [25] Yusuke Monno, Daisuke Kiku, Masayuki Tanaka, and Masatoshi Okutomi, "Adaptive residual interpolation for color and multispectral image demosaicking," *Sensors*, vol. 17, no. 12, pp. 2787–1–21, 2017.
- [26] Pierre-Jean Lapray, Luc Gendre, Alban Foulonneau, and Laurent Bigué, "Database of polarimetric and multispectral images in the visible and NIR regions," *Proc. of SPIE*, vol. 10677, pp. 1067738–1–14, 2018.

- [27] Xinhao Liu, Masayuki Tanaka, and Masatoshi Okutomi, “Practical signal-dependent noise parameter estimation from a single noisy image,” *IEEE Trans. on Image Processing*, vol. 23, no. 10, pp. 4361–4371, 2014.
- [28] Sofiane Mihoubi, Olivier Losson, Benjamin Mathon, and Ludovic Macaire, “Multispectral demosaicing using pseudo-panchromatic image,” *IEEE Trans. on Computational Imaging*, vol. 3, no. 4, pp. 982–995, 2017.